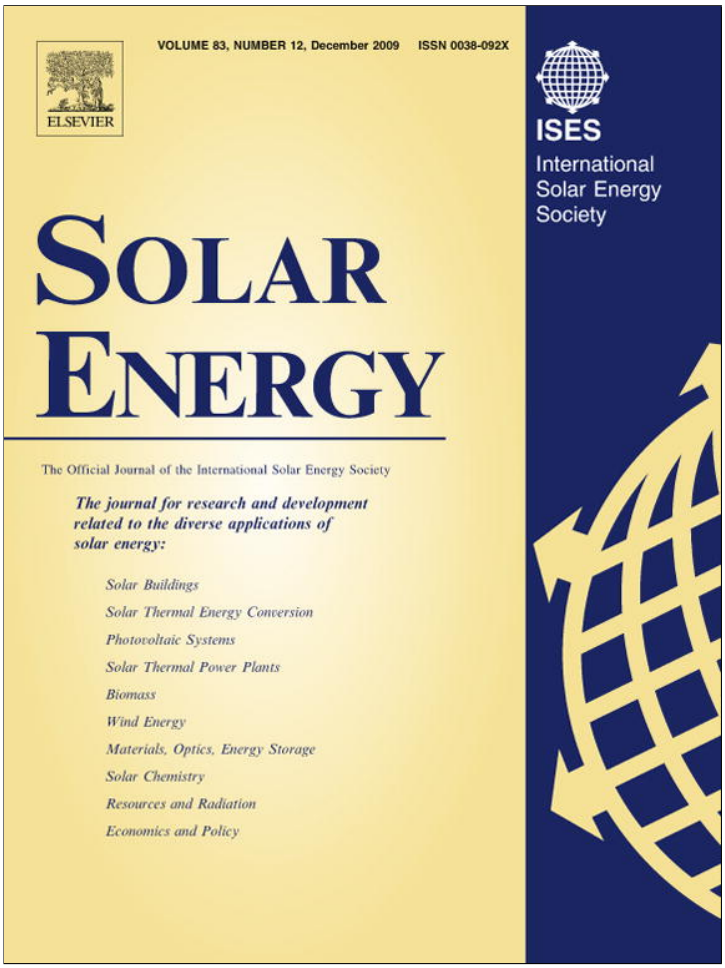

Available online at www.sciencedirect.com
ScienceDirect
Solar Energy 83 (2009) 2144–2156
SOLAR ENERGY
www.elsevier.com/locate/solener

# Improved broadband solar irradiance from the multi-filter rotating shadowband radiometer

J.J. Michalsky [a,*], J.A. Augustine [a], P.W. Kiedron [b]

[a] National Oceanic and Atmospheric Administration, Earth System Research Laboratory, 325 Broadway, Boulder, CO 80305, USA
[b] Cooperative Institute for Research in Environmental Sciences, University of Colorado, 325 Broadway, Boulder, CO 80305, USA

Received 16 March 2009; received in revised form 13 August 2009; accepted 18 August 2009
Available online 2 October 2009

Communicated by: Associate Editor Frank Vignola

**Abstract**

Approximations to total and diffuse horizontal and direct normal, broadband solar irradiance (280–4000 nm) can be obtained from the multi-filter rotating shadowband radiometer (MFRSR) using the unfiltered silicon channel of this seven-channel instrument. However, the unfiltered silicon channel only responds to wavelengths between 300 and 1100 nm and does not have a uniform spectral response. In contrast, the best, more expensive, first-class, thermopile-based radiometers respond fairly uniformly to all solar wavelengths. While the total horizontal and direct normal solar irradiance measurements made with the MFRSR unfiltered silicon channel are reasonable if carefully calibrated with a thermopile radiometer, the diffuse horizontal irradiance calibrated in this way has a large bias. These issues are common to all inexpensive, silicon-cell, solar pyranometers. In this paper we use a multivariate, linear regression technique for approximating the thermopile-measured total, diffuse, and direct broadband solar irradiances using the six, narrowband filters and the open-channel of an MFRSR. The calibration of the MFRSR for broadband solar by comparing various combinations of MFRSR channels to first-class thermopile instruments is illustrated, and methods to track the instrument response during field deployments are investigated. We also suggest an approach to calibrate the open-channel for all three components that could improve measurements that are made using typical, commercial, silicon-cell pyranometers.
Published by Elsevier Ltd.

*Keywords:* Multi-filter rotating shadowband radiometer; Silicon-cell pyranometer; Solar irradiance; Multivariate linear regression

## 1. Introduction

The use of the silicon-cell pyranometer for solar irradiance measurements is widespread because they are inexpensive compared to thermopile devices. Moreover, when they are used to measure total horizontal irradiance, their performance is acceptable for some applications if calibrated frequently. Many of the solar instrument manufacturers include a low-cost, silicon-cell pyranometer in their catalogues. The better of these devices operate similarly in that they incorporate a diffuser that receives solar radiation and transmits it to an underlying silicon detector beneath the diffuser. The diffuser acts to approximate the angular response of a perfect cosine receiver, i.e., the receiver's response should decrease exactly as the cosine of the angle of incidence.

One issue with simple, commercial silicon-cell pyranometers is that they are not temperature stabilized. Michalsky et al. (1987) and King and Myers (1997) give independent evidence for the Li-COR 200's increasing responsivity with rising temperature, and King and Myers (1997) provide a correction for Li-COR pyranometers based on temperature responses of seven Li-COR 200s. The multi-filter rotating shadowband radiometer (MFRSR), described in Harrison et al. (1994), uses a diffuser that transmits radiation to an unfiltered silicon-cell detector (open-channel) and to an additional six, 10-nm-wide, filtered channels that have

* Corresponding author. Tel.: +1 303 497 6360; fax: +1 303 497 6546.
*E-mail address:* joseph.michalsky@noaa.gov (J.J. Michalsky).

0038-092X/$ - see front matter Published by Elsevier Ltd.
doi:10.1016/j.solener.2009.08.007

central wavelengths near 415, 500, 615, 673, 870, and 940 nm. It operates by making a total irradiance measurement followed closely (a few seconds) by a shaded measurement of the diffuse, or scattered, sky irradiance. The direct solar irradiance is inferred by subtracting the diffuse measurement from the total value. One feature that sets the MFRSR apart from simple silicon-cell radiometers is that its detector is temperature stabilized near 40 °C, and, therefore, a temperature correction is not required.

The most significant issue with any silicon-cell pyranometer is that its spectral response is neither uniform nor inclusive of all the solar wavelengths. The response is low in the ultraviolet and blue, rises in the mid-visible wavelengths, and peaks in the near-infrared around 900 nm before falling sharply to a zero response near 1100 nm. The solar spectrum continues to wavelengths out to 4000 nm. While it is true that the energy in the spectrum beyond 1100 nm is reduced, it nevertheless accounts for 20–30% of the total energy in the shortwave when the sun is high in the sky. A minor issue is that most commercial silicon-cell pyranometers use a plastic diffuser that does not transmit wavelengths shorter than 400 nm, while the MFRSR transmits to the atmospheric cut-off around 300 nm.

If the relative spectral distribution of solar radiation did not change, i.e., the changes were simply multiplicative factors of the same spectral distribution, then the silicon-cell could be calibrated to correlate almost exactly with a uniform response sensor such as a thermopile pyranometer. It is the non-uniform spectral response of the silicon-cell detector to changing spectral distributions that causes the major calibration difficulties. For example, the clear diffuse sky is rich in blue whereas overcast-sky irradiance includes a more even distribution of all solar wavelengths. Therefore, if the silicon-cell pyranometer is calibrated using the total horizontal irradiance, it will significantly underestimate diffuse irradiance because the spectra of these two sources are dramatically different. An opposite, subtle effect occurs when measuring total horizontal irradiance at low-sun with an instrument that has been calibrated at high sun. When the sun is high, the solar signal is more uniform spectrally, whereas a low-sun signal is rich in the longer wavelengths, where the silicon-cell is more responsive. A measurement by a silicon-cell at low-sun, which is calibrated at high sun using a thermopile, yields a measurement that will be higher than that of a thermopile pyranometer because of the reddening of the spectrum for those conditions. Moreover, a difference in response of 2–3% is typical if the silicon-cell pyranometer is calibrated using total horizontal irradiance versus direct normal irradiance; the latter is slightly richer in the longer (redder) wavelengths. The direct normal calibration will appear to have a greater responsivity because the blue-sky irradiance is not part of the calibration source.

The primary motivation for this study was to determine whether the open-channel could be eliminated in order to use its position in the MFRSR head for another filter that could be used for other measurements. To that end, we use combinations of the spectral channels to calibrate the MFRSR for the best match to the total and diffuse horizontal and the direct normal shortwave broadband irradiance measurements. This paper considers the tradeoffs of including, or excluding, the open-channel among the channel combinations employed in the multivariate linear regressions used to calibrate the MFRSR for broadband solar components.

## 2. Multivariate linear regression

The strategy was to regress one, two, or three channels of the MFRSR against each thermopile-measured solar irradiance component, i.e., total horizontal, diffuse horizontal, or direct normal. All data are from the Atmospheric Radiation Measurement (ARM) Central Facility between Lamont and Billings, Oklahoma, at 36.605 °N and 97.485 °W. We applied the technique to data from two, co-located, but independent, MFRSRs. As stated earlier, no temperature correction is needed because MFRSRs are held near 40 °C. Additionally, departures from an exact cosine response were measured before the MFRSRs were deployed; corrections are applied to the diffuse horizontal and direct normal components, and the cosine-corrected total horizontal irradiance is calculated from these. Co-located with these MFRSRs are three sets of first-class thermopile pyranometers and pryheliometers that make simultaneous measurements of the three broadband solar components in question. The "best estimate" of total and diffuse horizontal and direct normal irradiance is selected from these three thermopile measurement sets following the procedure in Shi and Long (2002).

To find the optimum combination of filters to use for each component, we regressed each 'best estimate' thermopile component on four clear days against a linear combination of one, two, or three of the filters or the open-channel for every unique grouping of measurements,

$$best\_estimate = C_0 + C_1 * filterX + C_2 * filterY + C_3 * filterZ.$$

By comparing the standard deviations of the fits, we determined the best single filter or combination of filters (including the open-channel) to use for the clear-sky approximations. Table 1 lists results for multiple filter combinations, single channels, the open-channel, and some filter-open-channel combinations, separately, for total, direct normal, and diffuse irradiance. For the direct component, we forced the intercept through zero ($C_0$ was set at zero). This was necessary because the regression of the direct component was based predominantly on large irradiance values, which produced extrapolations to unreasonable non-zero intercepts. Table 1 entries are the root-mean-square differences (RMSDs) of the filter(s) approximations to the thermopile measurements, i.e.,

$$RMSD^2 = \sum_1^N (best\_estimate - C_0 - C_1 * filterX - C_2 * filterY - C_3 * filterZ)^2 / N.$$

Table 1
Root-mean-square differences in W/m$^2$ for approximations compared to thermopile first-class instruments for 1-min averages; comma-separated entries are for two, co-located MFRSRs; results are for two periods; four consecutive clear days and four consecutive partly cloudy to cloudy days. Mean parameter values for each period are given in first row of parameter investigated.

| Parameter, channels used | Clear | Partly cloudy |
|---|---|---|
| Total horizontal | Mean = 534.8 | Mean = 488.3 |
| 3-Channels (415, 673, 940) | 2.4, 3.6 | 24.8, 23.5 |
| 2-Channels (673, 940) | 2.4, 4.1 | 25.1, 24.3 |
| 1-Channel (615) | 6.3, 6.7 | 41.0, 39.2 |
| 1-Channel (open) | 4.5, 4.9 | 25.4, 24.1 |
| 3-Channels (open, 673, 940) | 2.2, 3.8 | 25.4, 24.2 |
| Direct normal | Mean = 802.9 | Mean = 435.7 |
| 3-Channels (500, 870, 940) | 10.4, 9.9 | 39.2, 42.1 |
| 2-Channels (500, 870) | 14.7, 14.2 | 46.5, 46.4 |
| 1-Channel (673) | 24.1, 31.4 | 49.4, 51.8 |
| 1-Channel (open) | 10.0, 14.3 | 40.5, 42.9 |
| 3-Channel (open, 673, 940) | 8.8, 10.1 | 39.3, 42.8 |
| 2-Channel (open, 615) | 9.1, 10.4 | 40.7, 43.3 |
| Diffuse horizontal | Mean = 65.4 | Mean = 187.3 |
| 3-Channels (415, 673, 940) | 1.0, 1.7 | 16.9, 19.2 |
| 2-Channels (415, 615) | 1.0, 1.8 | 19.7, 21.0 |
| 1-Channel (500) | 1.6, 2.2 | 34.5, 33.2 |
| 1-Channel (open) | 3.1, 2.8 | 90.8, 81.0 |
| 3-Channels (open, 415, 615) | 1.0, 1.8 | 18.1, 18.9 |

Table 1 contains results for two different MFRSRs, whose RMSDs are separated by commas in column 2 for clear days, and in column 3 for partly cloudy days, and for each component as labeled. Approximate central wavelengths for the filters are given in parentheses.

The one-filter estimates give the poorest fits except for the open-channel estimate of diffuse horizontal irradiance. On the other hand, the open-channel estimates of total horizontal and direct normal irradiances are comparable to the two and three-filter estimates. The RMSDs using two versus three-filters are nearly the same suggesting that using more channels would not result in significantly better agreement, i.e., most of the variance can be explained by two or three properly-chosen, filters. Results for the two MFRSRs shown in the table are not identical, but are similar in magnitude. These slight differences for the same type of instrument are expected for reasons that include, minor filter differences, small timing and alignment differences, etc.

Sampling and sensor-response issues cause large RMSDs for the partly cloudy sky cases in column 3 of Table 1. The sampling rates of the MFRSRs and thermopile radiometers are not identical. The thermopile instruments sample every 2 s, therefore, there are 30 samples in the 1-min averages that are calculated. The MFRSR shadowband cycle produces a measurement of the three components every 20 s, resulting in three samples per minute at 20, 40, and 60 s. Of course, on partly cloudy days when the solar signal varies considerably over short periods of time, there will be a large variance caused by these incongruent sampling modes. Additionally, a portion of the variance is caused by the differences in response times of the thermopile, which is on the order of seconds, and the silicon detector, which is on the order of microseconds.

Table 2 contains the data from the same four clear and the same four cloudy days as in Table 1, but in this table the entries are based on 15-min averages. There are slight differences in the average irradiances for the parameter compared to Table 1 because not all of the 1-min data are contained in the 15-min averages. For example, one missing data point in a 15-min period would result in that 15-min average not being used. The improvements in RMSDs are small for the clear days in column two of Table 2 compared with column 2 of Table 1 as one might expect for stable conditions. However, the RMSDs for 15-min average, partly cloudy conditions (in column three of Table 2) are one-fourth to one-third as large as the RMSDs for 1-min averages under partly cloudy conditions (column three of Table 1). The exceptions to this are the minor reductions in RMSDs for the one-filter regressions for all parameters and the open-channel regression for the diffuse. These improvements are small because large biases remain and these produce large RMSDs; these issues will be discussed further below.

As seen in Table 1, the RMSDs for combinations that include the open-channel are often better than other combinations for clear days (column 2), but are often not as good for partly cloudy days (column 3). The best agreement with broadband thermopile measurements is for approximations based on three-filter estimates, but the improvement is marginal over two-filter estimates. The open-channel estimates of total horizontal and direct

Table 2
Root-mean-square differences in W/m$^2$ for approximations compared to thermopile first-class instruments for 15-min averages; comma-separated entries are for two, co-located MFRSRs; results are for two periods; four consecutive clear days and four consecutive partly cloudy to cloudy days. Mean parameter values for each period are given in first row of parameter investigated.

| Parameter, channels used | Clear | Partly cloudy |
|---|---|---|
| Total horizontal | Mean = 528.9 | Mean = 511.1 |
| 3-Channels (415, 673, 940) | 2.2, 3.6 | 7.4, 6.6 |
| 2-Channels (673, 940) | 2.3, 4.0 | 6.7, 6.4 |
| 1-Channel (615) | 6.0, 6.6 | 34.2, 32.3 |
| 1-Channel (open) | 4.3, 4.8 | 7.1, 6.5 |
| 3-Channels (open, 673, 940) | 2.0, 3.7 | 7.4, 6.0 |
| Direct normal | Mean = 807.4 | Mean = 465.4 |
| 3-Channels (500, 870, 940) | 7.1, 6.5 | 11.2, 9.2 |
| 2-Channels (673, 940) | 13.0, 11.3 | 12.7, 18.0 |
| 1-Channel (673) | 22.7, 30.5 | 30.6, 29.5 |
| 1-Channel (open) | 7.3, 12.3 | 13.5, 11.3 |
| 3-Channel (open, 673, 940) | 6.6, 8.3 | 10.7, 9.9 |
| 2-Channel (open, 615) | 6.1, 7.7 | 13.0, 12.5 |
| Diffuse horizontal | Mean = 65.2 | Mean = 188.8 |
| 3-Channels (500, 615, 870) | 0.9, 1.5 | 9.5, 18.8 |
| 2-Channels (415, 673) | 0.7, 1.4 | 8.6, 14.8 |
| 1-Channel (500) | 1.3, 1.9 | 30.7, 28.1 |
| 1-Channel (open) | 2.4, 2.0 | 91.6, 80.3 |
| 3-Channels (open, 415, 940) | 0.7, 1.4 | 9.8, 23.2 |

normal irradiances are comparable to multi-filter estimates, but the diffuse horizontal irradiance estimate based on the open-channel regression is useless for cloudy skies. In general, the regressions that include the open-channel are no better than the filter-only regressions, and there is no compelling reason to retain the open-channel for estimating solar total, diffuse, and direct irradiance from an MFRSR.

## 3. Results and discussion

### 3.1. Total horizontal irradiance

Fig. 1(a) contains three plots of the total horizontal irradiance including the best estimate (thermopile) data (in black), an approximation based on a regression of the 615-nm filter data (in green) and an approximation based on a regression of the 673 and 940-nm filters data (in red) for four clear days. The 615-nm filter produced the lowest standard deviation of any single MFRSR filter regression. Its regression-model results agree well with best estimate data except for a subtle underestimate around noon of the second day. The scatterplot of thermopile data versus the 615-approximation in Fig. 1(b) further demonstrates this good agreement. The slope one (perfect agreement) line in green appears to exactly overlay the red line, which is the least squares fit of the 615-approximation to thermopile data. The slope, correlation coefficient, mean difference, and root-mean-square difference (RMSD) are printed on the plot. Fig. 1(c), which is a scatterplot of the 615/940-filter approximation versus the thermopile measurement, looks similar to 1(b), but the RMSD is 60% smaller. In Fig. 1(d) the fitting coefficients used in Fig. 1(a) are used to approximate the data for four consecutive days that are partly cloudy with a few totally overcast

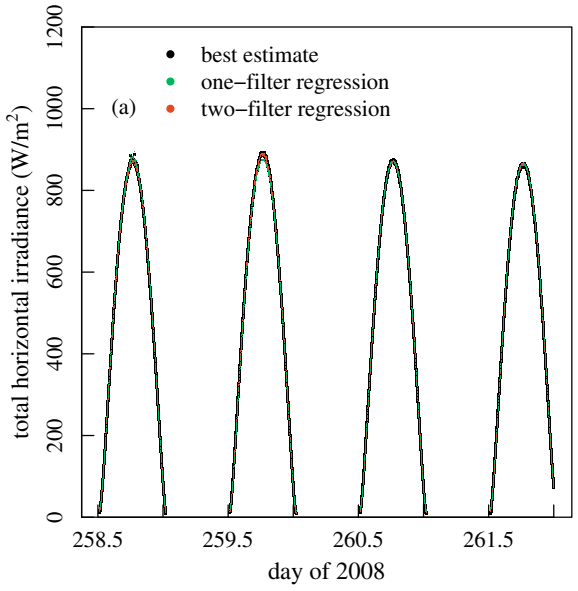


Fig. 1a. The best estimate total horizontal irradiance measured by the thermopile instruments is plotted in black. The linear, least squares fit that gave the smallest standard deviation to the thermopile data for four clear days using a single filter regression was the 615-nm channel plotted in green. The agreement is very good except for the slight underestimate for the second day's noon values. The thermopile data are nearly overplotted by red-point approximations that use two-filters, one centered near 673 and the other near 940 nm. Notice the improvement at noon of the second day. (For interpretation of the references to colour in this figure legend, the reader is referred to the web version of this article.).

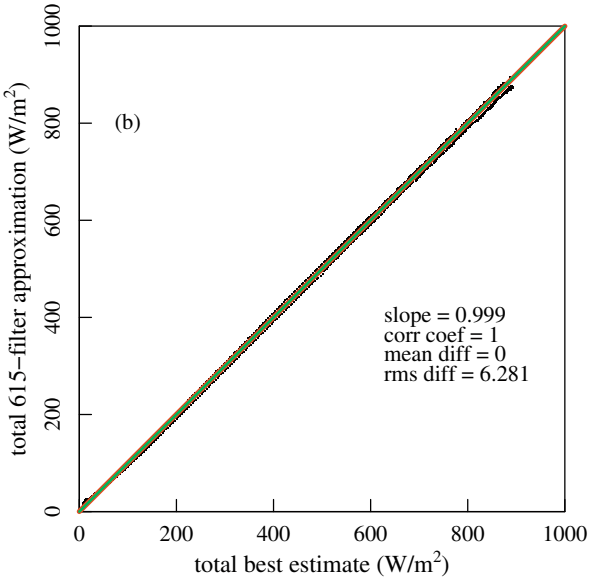


Fig. 1b. The scatterplot of the 615-nm least squares fit approximations versus the best estimate thermopile data in Fig. 1(a); the numbers in the lower right of the figure include the slope of the linear least squares fit to the data, the correlation coefficient, and in units of W/m$^2$, the mean difference, and the root-mean-square-difference (RMSD) from perfect agreement with the thermopile total horizontal irradiance values. The wide red line is the fit and the green narrow line represents perfect correlation. (For interpretation of the references to colour in this figure legend, the reader is referred to the web version of this article.).

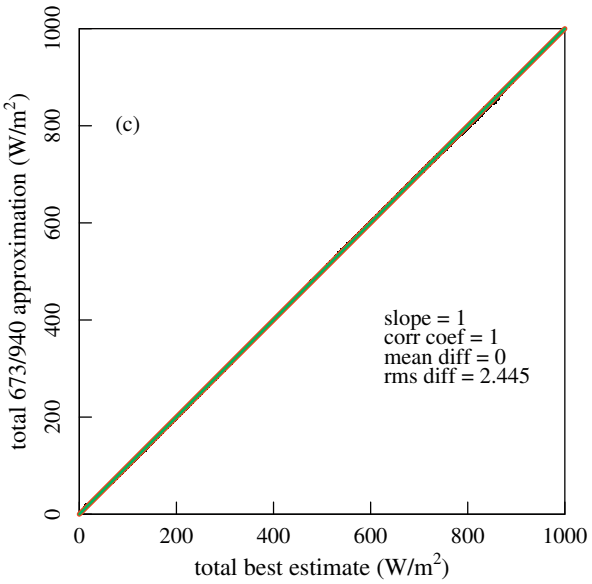


Fig. 1c. The scatterplot of the 673/940-nm least squares fit approximation to the best estimate thermopile data in Fig. 1(a); note the considerable improvement in the RMSD.

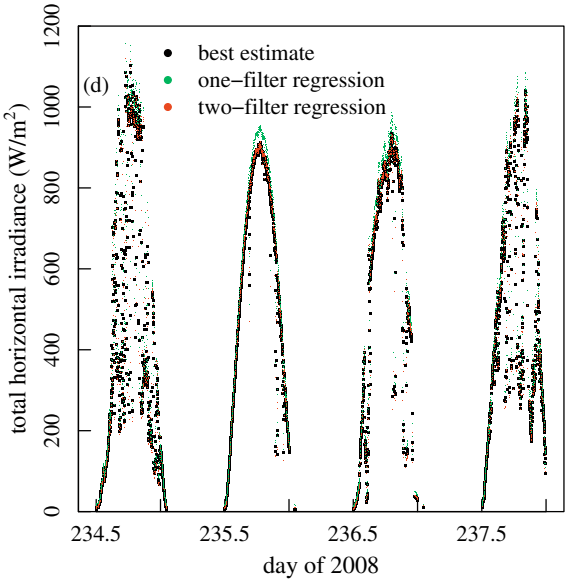


Fig. 1d. The fitting coefficients, determined from the data in Fig. 1(a), are applied to four consecutive partly cloudy days. The thermopile values are in black, the one-filter (615 nm) approximation, which is too high, is in green, and the two-filter (673/940 nm) approximation, which fits the black points well, is in red. (For interpretation of the references to colour in this figure legend, the reader is referred to the web version of this article.).

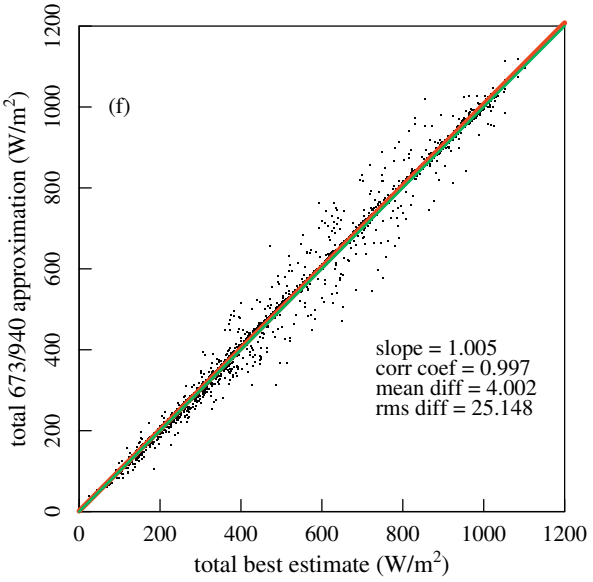


Fig. 1f. The scatterplot of the 673/940-nm fit on the partly cloudy days has a slope within 1% of unity, a mean difference of 4.0 W/m$^2$, and a RMSD that is noticeably smaller than the RMSD in Fig. 1(e). Sampling issues that are discussed in the text and in the caption for Fig. 1(e) can explain most of the scatter.

periods. The 615-filter approximation (in green) is generally higher than the best estimate thermopile measurements, which is clearly demonstrated in the scatterplot in Fig. 1(e). This can be explained by considering that the

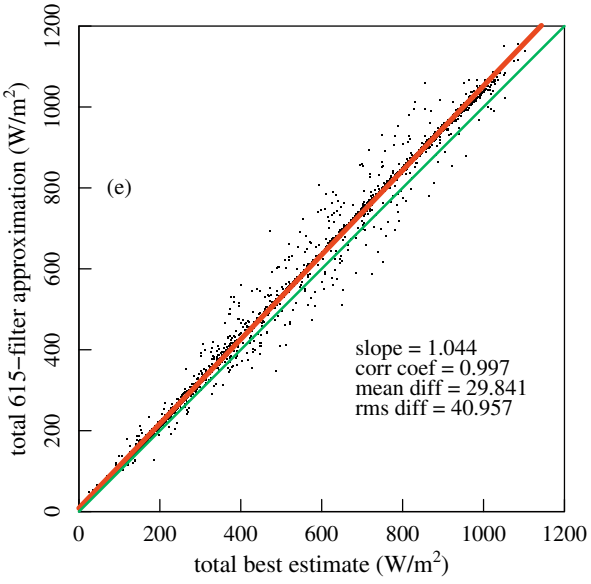


Fig. 1e. The slope and mean difference for the 615-nm fit for these partly cloudy days indicate a consistent overestimate of total horizontal irradiance. The slope is greater than unity because the water–vapor on the clear days was low (1.5–2.0 cm) compared to the cloudy days (3.5–4.0 cm), and the 615-nm filter is not sensitive to water–vapor, therefore, there is no adjustment for the larger column of water–vapor on these days. The RMSD is large because of the large mean difference, and because of sampling issues. These 1-min data points include 30 samples for the thermopile, 1-min average and 3 samples for the MFRSR, 1-min average.

615-nm filter measures in a region of the solar spectrum that is affected by aerosol extinction, Rayleigh scattering, and Chappuis-band ozone absorption, while the broadband is affected by these elements plus water–vapor and other minor species. Since the water–vapor is lower on the clear, dry days used for calibration (the column water–vapor as measured by a microwave radiometer was typically between 1 and 1.5 cm on the four clear days used), applying those calibrations on higher water–vapor days such as the partly cloudy days in Fig. 1(d) (the column water–vapor was typically between 3.5 and 4 cm for these 4 days) produces irradiance overestimates. This explains the approximated data fit (red line) having a higher slope than the perfect correlation (green) line in Fig. 1(e). The 673/940-approximation in the red overplots the black thermopile values rather well in Fig. 1(d). This is further illustrated with the nearly one-to-one, redline fit in Fig. 1(f). The 940-nm filter captures the additional variance caused by water–vapor. Using three channels slightly improves the results, but the differences would not be detectable in similar plots, and, therefore, are not shown.

Figs. 2(a) and 2(b) examines how well the unfiltered open silicon channel alone can approximate total horizontal irradiance. Again, this is somewhat different from comparing to a simple silicon-based pyranometer because the MFRSR open detector is temperature stabilized, the cosine response is corrected, and the spectral response between 300 and 400 nm is included. Both panels of Figs. 2(a) and 2(b) compare well with the dual-channel results shown in panels (c) and (f) of Figs. 1(a)–1(f), with RMSDs negligibly larger than those in Figs. 1(c) and 1(f). These excellent results suggest that the MFRSR open-channel, with

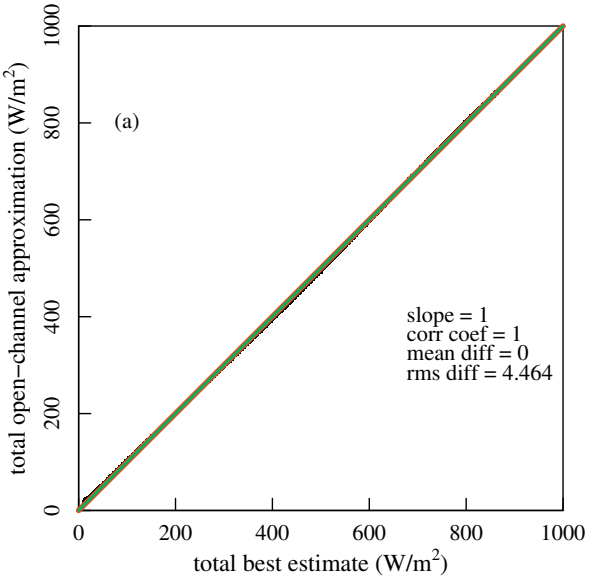


Fig. 2a. In this plot the unfiltered silicon (open) channel approximation is plotted against the best estimate total horizontal irradiance for the clear day. Comparing the RMSD to Fig. 1(b) and (c) we notice an intermediate result.

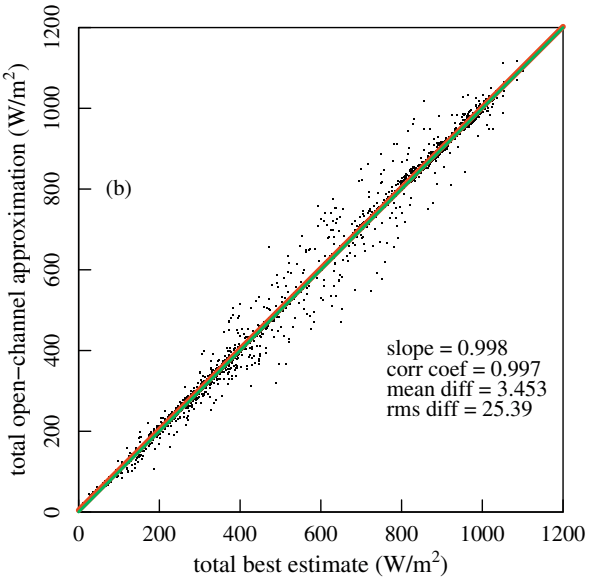


Fig. 2b. The partly cloudy days' scatterplot of the open-channel fit to the best estimate thermopile data has almost the same RMSD as the two-filter fit in Fig. 1(f).

its detector temperature held constant and cosine-corrected direct and diffuse components, reproduces thermopile measurements of total horizontal irradiance well for both clear and cloudy skies.

### 2.2. Direct normal irradiance

For the linear regressions involving direct beam irradiance the intercept was forced to zero because most of the clear-sky data values that the regression was based on were

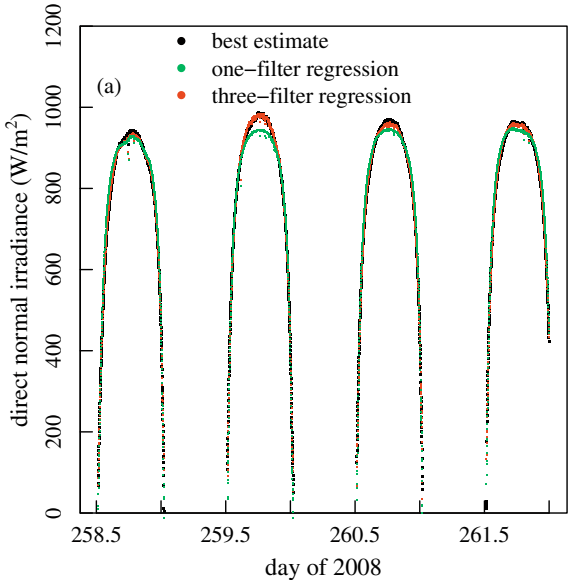


Fig. 3a. As before the thermopile data are in black. These are direct normal irradiances for the same four clear days. The 673-nm filter approximation (green points) underestimates the peak values while the 500/870/940-nm approximation is better. (For interpretation of the references to colour in this figure legend, the reader is referred to the web version of this article.).

large, and this led to unreasonable, non-zero intercepts. For the direct normal component the filter near 673 nm gave the smallest RMSD of any single filter regression model. For three-filter combinations, 500, 870, and 940 nm gave the smallest RMSD. For clear days, Fig. 3(a), noontime approximations of the direct beam are underestimated and the mid-range values are overestimated by the 673-filter approximation. This is more clearly seen in the scatterplot in Fig. 3(b).

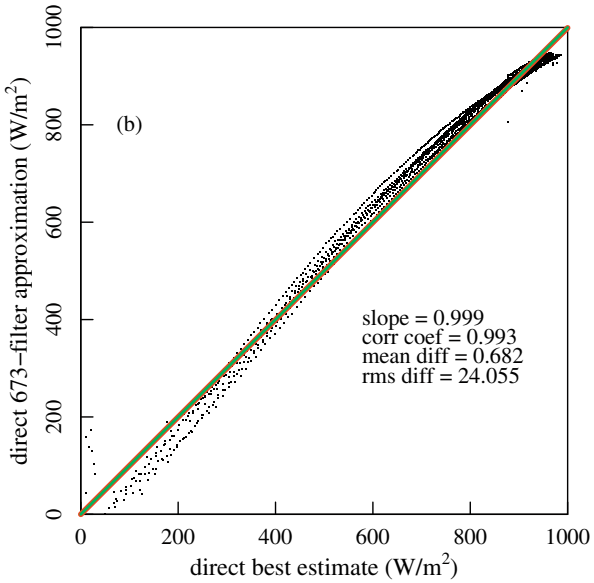


Fig. 3b. This scatterplot indicates that the 673-nm approximation underestimates intermediate direct irradiances and overestimates the lowest and highest values. In this plot the fit is forced to zero because the preponderance of large direct values yields a non-zero intercept.

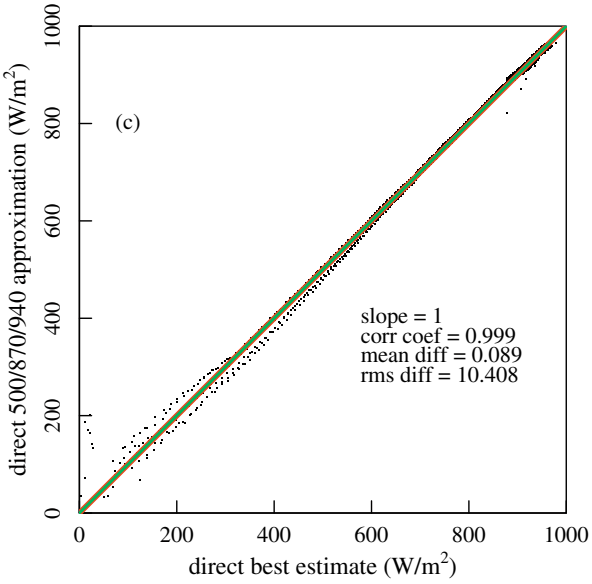


Fig. 3c. The three-parameter fit using 500/870/940-nm filters is a much better approximation to the thermopile direct normal irradiance than the 673-nm filter indicated by the improvement in the RMSD in this scatterplot.

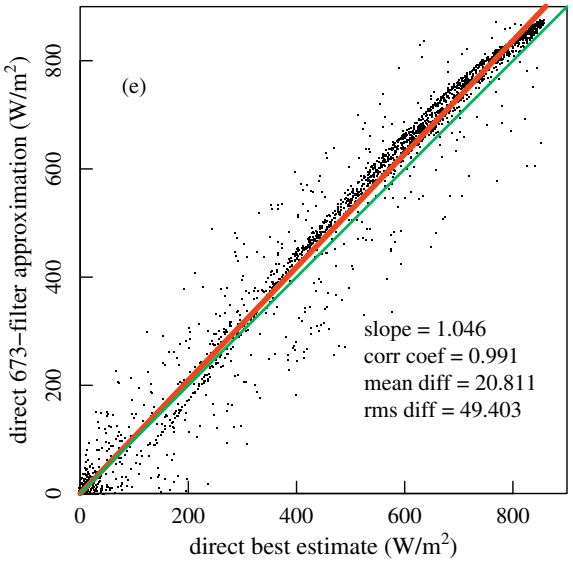


Fig. 3e. In this scatterplot the one-filter approximations overestimate the thermopile data by about 5%. As in the explanation of Fig. 1(e), a 673-nm filter that does not contain water–vapor absorption does not explain water–vapor-affected irradiance.

The 500/870/940-filter approximation (red points in Fig. 3(a)) agrees well with the black thermopile points. This is confirmed in Fig. 3(c) where there is close agreement with the green perfect correlation line. For partly cloudy days, shown in Fig. 3(d)–3(e), the one-filter approximation overestimates the measured direct irradiance for the same reason that total irradiance was overestimated using a single-channel approximation, i.e., the water–vapor is low on the clear days that were used to derive the regression model. Higher water–vapor on partly cloudy days would decrease the direct normal signal, but since there is no absorption by water–vapor in the 673-nm signal, the approximated value is uninformed with respect to water–vapor resulting in an erroneously high direct irradiance. In Figs. 3(d) and 3(f) the three-filter approximation produces a better fit to partly cloudy data. There are no pronounced high and mid-range mismatches in Figs. 3(d) and 3(f) as seen in the single-channel plots Figs. 3(d) and 3(e). A two-filter parameterization using 673- and 940-nm filters (not shown) produces nearly the same results. In Figs. 4(a) and 4(b) only the open-channel is used to obtain a best fit to the thermopile, best estimate

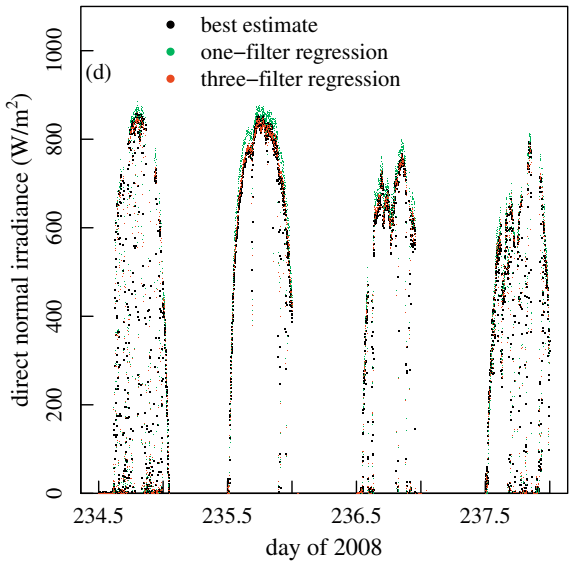


Fig. 3d. For the partly cloudy days the one-filter approximations overestimate the thermopile best estimates for direct while the three-filter approximations better estimate the thermopile direct although the scatter is large because of sampling issues as discussed earlier.

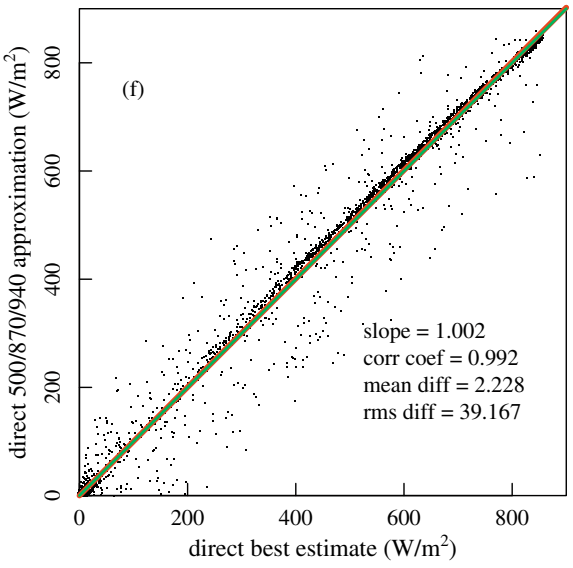


Fig. 3f. The three-filter approximations better match the thermopile data although much scatter remains because of sampling differences.

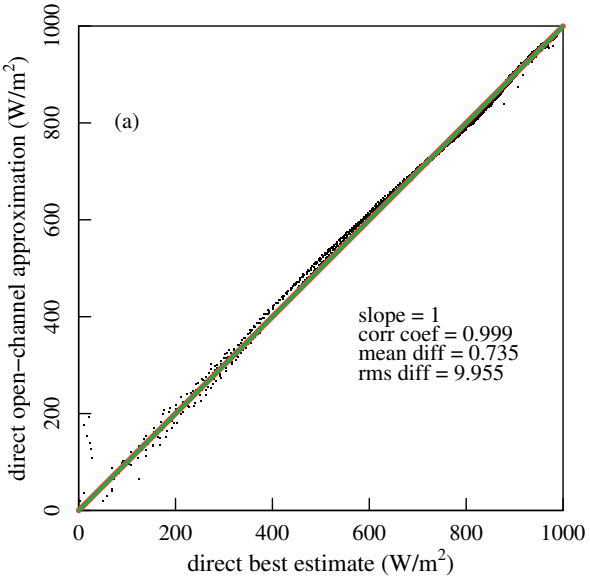


Fig. 4a. The scatterplot of the open-channel fit to the clear-day thermopile direct is comparable to the three-filter fit in Fig. 3(c).

direct normal irradiance. The results in Figs. 4(a) and 4(b) closely mimic the three-filter results in Figs. 3(c)–3(f).

If a temperature stabilized open silicon channel is used, the total horizontal and direct normal irradiances would be approximated well by a simple regression relationship between the silicon-cell open-channel and the thermopile instruments. However, the calibration constants (or, inversely, the responsivities) derived from the fits will be different for total and direct. Generally, the responsivity for the total horizontal irradiance is smaller than that for the direct normal by about 2.5%. This is expected because the direct normal irradiance does not contain the blue-sky diffuse short wavelength radiation that the total horizontal irradiance includes. The silicon detector is less sensitive to the short wavelength radiation, resulting in a diminished response for total horizontal compared to the somewhat redder direct normal spectrum.

### 3.2. Diffuse horizontal irradiance

If we regress one, two, or three-filters or the open-channel versus the best estimate thermopile data on clear days we can, as seen for the diffuse horizontal parameter in Table 1 column 2, estimate diffuse quite well with the filter regressions, and less accurately with the open-channel approximation yielding a RMSD of about 5%. If one uses the coefficients from these fits for the partly cloudy days, the two- and three-filter fits give considerably lower RMSDs as seen in Table 1 than the single filter or open-channel results. These partly cloudy results are illustrated in Figs. 5(a)–5(c) for one-filter, open-channel, and three-filter regressions, respectively.

The results in Figs. 5(a) and 5(b) can be explained by the change in the spectral energy distribution of diffuse irradiance on the clear days that are used for the regression calibration relative to the diffuse spectral energy distribution on cloudy or partly cloudy days. To aid in this understanding, Fig. 6 shows the spectral distribution for the *total* solar irradiance at the surface on a clear day (black curve), which has nearly the same spectral distribution as the *diffuse* irradiance of a cloudy sky (apart from a scaling factor). So, for this discussion, the black curve in Fig. 6 represents the relative spectral distribution of a *cloudy diffuse sky*.

The *clear-sky diffuse* spectrum (blue curve) is sharply skewed toward the short wavelengths and peaks around 400 nm. The blue curve in Fig. 6 is multiplied by 5.6 to better show the relative spectral differences between clear and

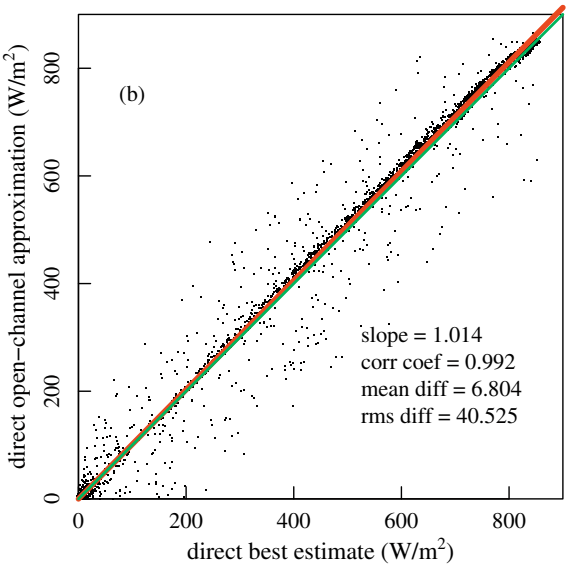


Fig. 4b. The partly cloudy direct beam open-channel estimates match the thermopile values about as well as the three-filter fit in Fig. 3(f).

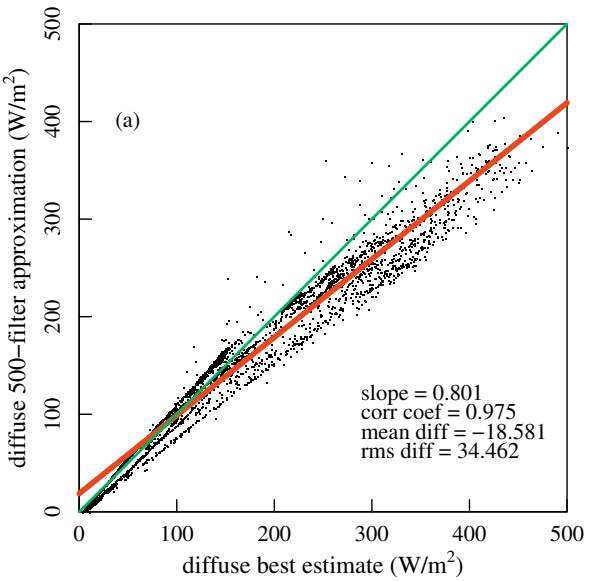


Fig. 5a. Using the 500-nm calibration from clear days, the partly cloudy days' diffuse is primarily underestimated. The explanation is given in the text.

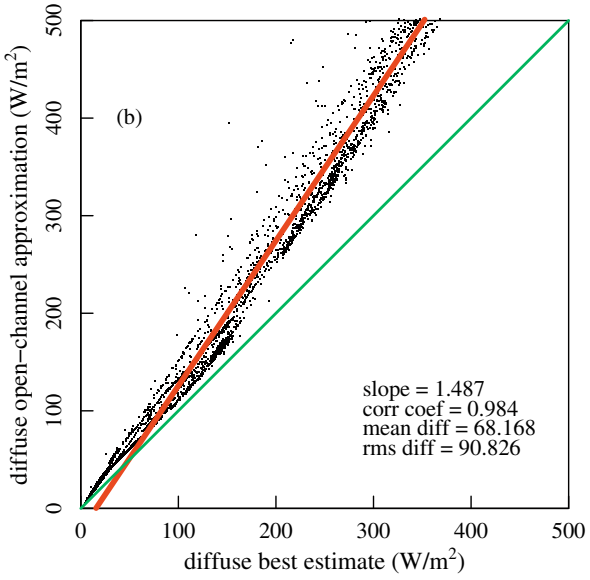


Fig. 5b. This scatterplot of the open-channel approximations for diffuse on partly cloudy days indicates the preponderance of overestimated data, including a large mean difference and large RMSD. The explanation is given in the text.

cloudy diffuse irradiance and to produce almost the same irradiance in the 500-nm filter, whose full width at half maximum is represented by the green vertical lines. If the 500-nm filter were calibrated using the blue spectrum, it would predict the integral of the blue spectrum as the estimate for diffuse irradiance and be correct, however, a cloudy-sky spectrum that gave the same 500-nm reading would be the integral of the black curve that is a higher irradiance. Consequently, this calibration procedure under predicts diffuse irradiance as seen in Fig. 5(a).

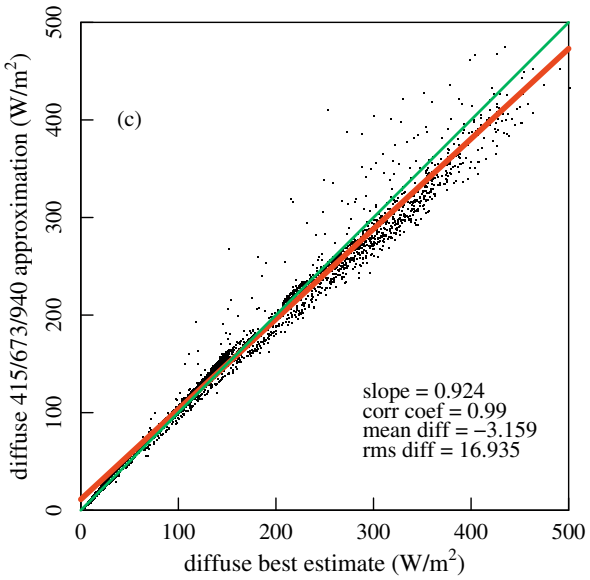


Fig. 5c. The thermopile, diffuse horizontal irradiance on partly cloudy days is better approximated using a three-filter (415, 673, and 940 nm) fit to the data. The agreement, however, is less satisfying than it was for three-filter fits to total horizontal and direct normal irradiance.

The differences in the spectral makeup of the diffuse solar signal at the surface under clear and cloudy diffuse skies, combined with the spectral response of silicon (red curve in Fig. 6) cause problems when attempting to calibrate the open silicon-cell for diffuse measurements. The calibration under clear skies is represented by the intersection of the red and blue curves in Fig. 6, whereas measurements of cloudy skies are represented by the intersection of the red and black curves (greater area). Partly cloudy conditions represent something in between these two extremes, but it is always greater than the clear-sky case that the regression calibration represents. The result is that a partly cloudy measurement always senses more energy than the clear-sky calibration would predict. Fig. 5(b) demonstrates that the differences discussed above result in overestimates of the predicted diffuse for cloudy to partly cloudy conditions.

If we use two or three channels to approximate the clear-sky diffuse irradiance, the partly cloudy day comparisons improve considerably. Fig. 5(c) illustrates this multivariate fit to three-filters centered near 415, 673, and 940 nm, which gave the best three-filter results. The two-channel results using 415 and 615 nm do almost as well (see Table 1). Including the open-channel in a three-parameter fit produces about the same RMSDs as the three-filter fit in Table 1.

As is evident from Fig. 5(b), approximating the thermopile-measured diffuse horizontal irradiance on partly cloudy days using regressions on clear days for the open-channel did not produce useful results. However, the good agreement between the open-channel approximations of direct normal and total horizontal irradiance compared to thermopile measurements (Figs. 2(a), 2(b), 4(a), and 4(b)) suggests that the diffuse irradiance calculated from the difference of the total and direct approximations may produce a better estimate of diffuse than that in Fig. 5(b). The direct normal irradiance must be multiplied by the cosine of the solar-zenith angle before subtracting from the total horizontal to calculate diffuse. Fig. 7(a)–7(c) illustrates the difference between using a clear-sky diffuse regression (a) and calculating the difference between total and direct to get diffuse (b) for clear skies. These scatterplots for clear-sky diffuse comparisons are similar with the diffuse based on differencing having a larger RMSD because of the $-2.9\ W/m^2$ offset; there is zero offset in Fig. 7(a) using regression. The slight increase in RMSD for clear skies when a difference is used is more than compensated when we compare Figs. 5(b) and 7(c) for partly cloudy skies. The partly cloudy sky estimates are vastly improved in Figs. 7(c) over 5(b), the latter based only on clear-sky regression, and Fig. 7(c) is similar to the three-filter regression results of Fig. 5(c).

To investigate this approach further, we estimate diffuse by calculating the differences using the best three-filter estimates of total horizontal and of direct normal irradiance. The results in Fig. 8(a) for clear days are comparable to the results in Figs. 7(a) and 7(b). Likewise, Fig. 8(b) for

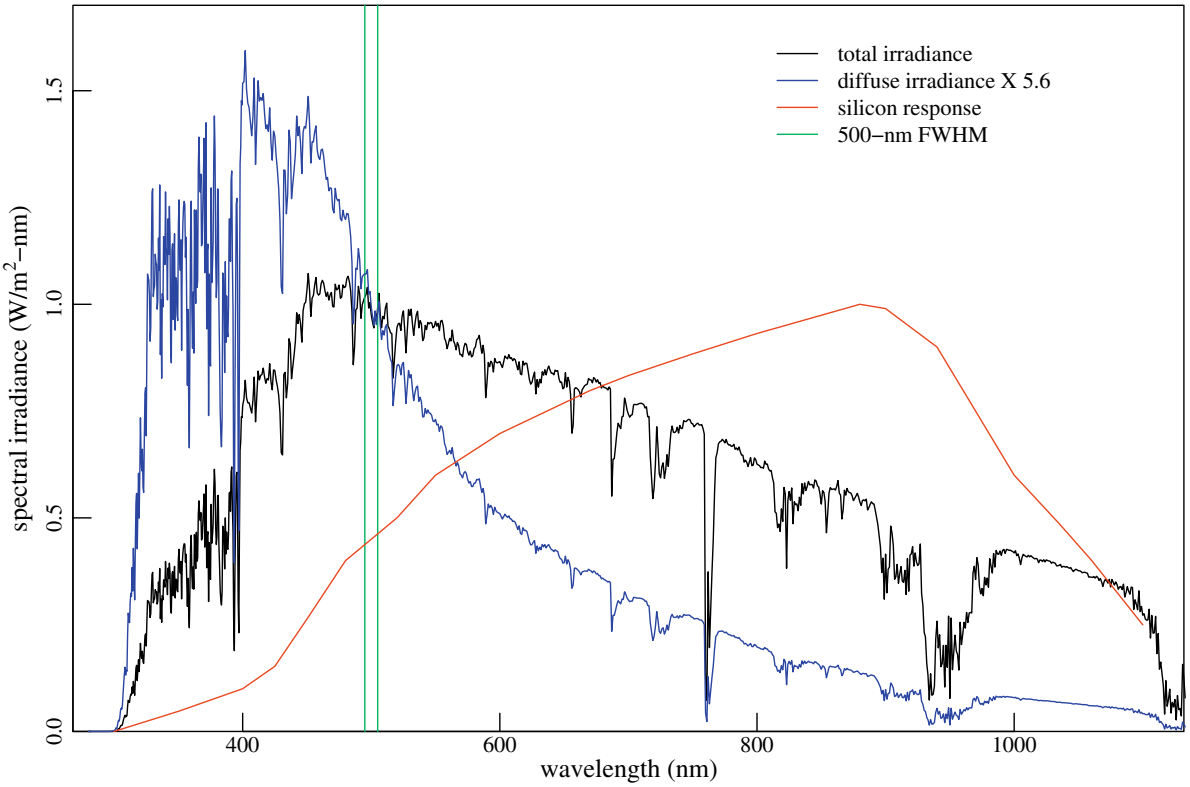


Fig. 6. This figure illustrates the spectral differences between total horizontal full solar spectrum, which has about the same spectral distribution as cloudy skies (apart from a scaling factor), and clear-sky diffuse irradiances, which are shifted to short wavelengths. The full width at half maximum for a typical 500-nm channel is shown as two vertical green lines. To match the 500-nm irradiance of the total horizontal spectrum, the diffuse has to be multiplied by 5.6; the forced agreement at 500 nm demonstrates that a calibration based on clear-sky spectra will underestimate cloudy or partly cloudy sky diffuse irradiance. Compare the area under the blue and black spectra. The relative silicon spectral response is plotted in red. A calibration based on observing a blue-sky spectrum with a silicon response will produce a low responsivity that is accurate when observing blue-sky spectra, but leads to overestimates of irradiances that contain the full solar spectrum. Compare the intersection of the red silicon response with the blue and then the black spectra. (For interpretation of the references to colour in this figure legend, the reader is referred to the web version of this article.).

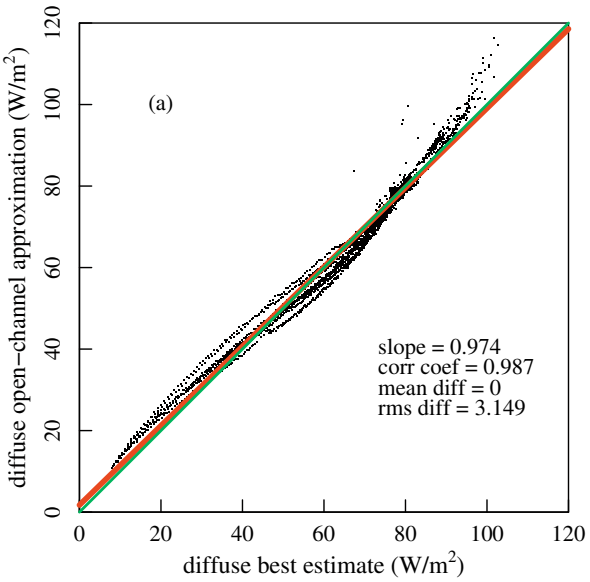


Fig. 7a. In this plot the open-channel diffuse estimate is obtained by calibrating the open-channel using a regression for clear skies; this produces fair agreement with thermopile diffuse values for these conditions as illustrated in this scatterplot.

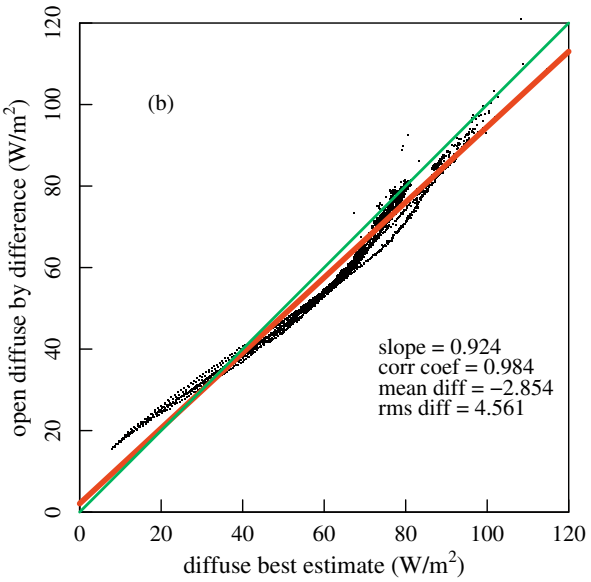


Fig. 7b. In this scatterplot the open-channel diffuse is obtained by subtraction of the direct irradiance on a horizontal surface from the total irradiance; the RMSD is only slightly larger than in Fig. 7(a) for these clear-sky conditions.

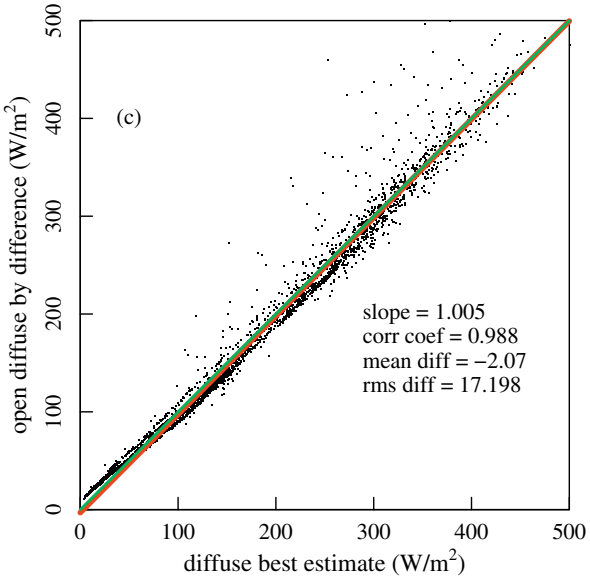


Fig. 7c. In this scatterplot for partly cloudy days the diffuse by subtraction is in much better agreement with the thermopile data than seen in Fig. 5(b), which is based on open-channel regression of clear-sky data. The slope is nearly one with a small mean difference and a RMSD that is one-fifth as large as in Fig. 5(b).

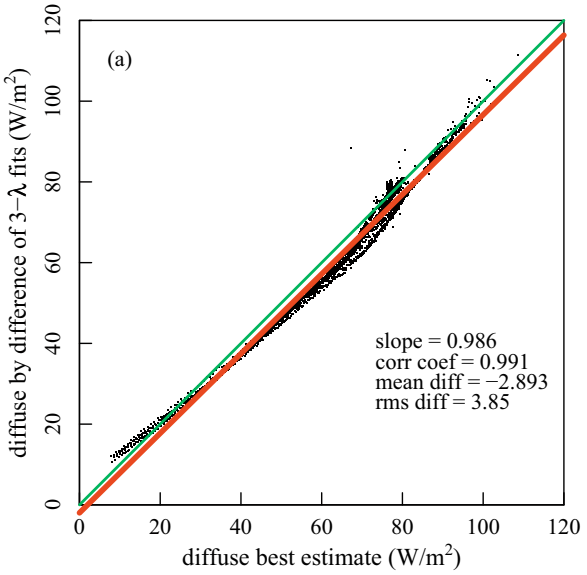


Fig. 8a. In this scatterplot the approximated diffuse for clear skies is calculated by subtracting the best estimate direct on the horizontal, based on three-filter fits, from the total horizontal estimate based on three-filter fits. The results are similar to Figs. 7(a) and (b).

partly cloudy days is similar to Figs. 5(c) and 7(c). All of these differencing and multi-filter regressions produce estimates with similar RMSDs.

## 4. Summary

The multivariate regression approach to approximating solar broadband shortwave irradiance components outlined in this paper demonstrates that narrowband-filter measurements from an MFRSR can explain most of the variance and, therefore, produce reasonable estimates with small mean differences of the diffuse and total horizontal and direct normal irradiance. Optimal combinations of filters were determined through regression analyses involving all combinations of all filters, including the open-channel. We found that two- and three-filter estimates produce very good and similar results, and that adding more filters yielded negligible improvement. For example, although a six-filter regression model for direct normal clear-sky irradiance reduced the RMSD to 9.3 W/m$^2$ versus 10.6 W/m$^2$ for a three-filter model, for partly cloudy-skies the RMSD for six filters was 39.0 W/m$^2$ versus 38.7 W/m$^2$ for three-filters.

A goal of this study was to determine whether the open (unfiltered) channel could be eliminated in favor of another useful application. Including the open-channel with one or two narrowband channels in the regression analysis often produced the smallest RMSD for clear-sky simulations, but this combination often yielded slightly higher RMSDs for partly cloudy conditions (see Table 1). Therefore, using the open-channel in combination with other filters is not essential for good approximations of the broadband solar components.

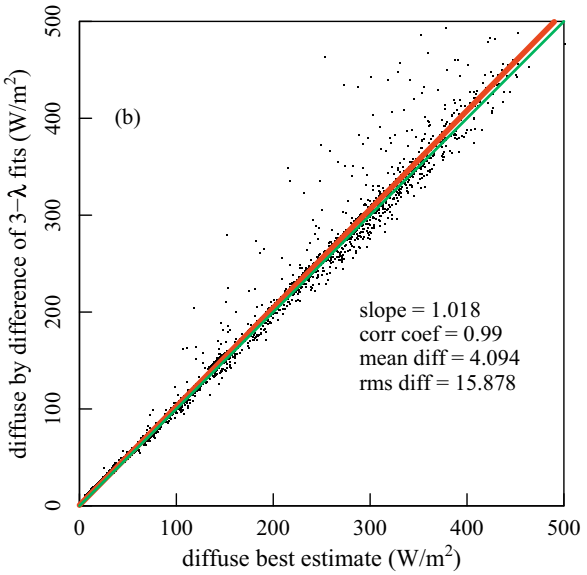


Fig. 8b. This is similar to Fig. 8(a) except for partly cloudy skies. These results are similar to Fig. 7(c).

Table 3 indicates the ten best fits in terms of standard deviations (1$\sigma$) for two- and three-channel combinations on the four clear days. The emboldened and underlined entries indicate the best three-filter candidates for each component. The two-filter fits that do almost as well at approximating the component are emboldened and underlined, as well. Examining Table 3, it is apparent from the negligible increase in the standard deviations of the fits ($\sigma$ columns) that, if some filters are not available, suitable substitutes can be found.

Table 3
The ten best fits in terms of lowest standard deviations ($\sigma$ in W/m$^2$) for two- and three-filter fits for each solar irradiance component; the exception is that the first 15 entries in the direct 3-channel fits involve the open-channel plus two-filters.[1]

| Total (3 λs) | σ | Total (2 λs) | σ | Direct (3 λs) | σ | Direct (2 λs) | σ | Diffuse (3 λs) | σ | Diffuse (2 λs) | σ |
|---|---|---|---|---|---|---|---|---|---|---|---|
| Open/673/940 | 2.22 | **673/940** | 2.45 | Open/673/940 | 8.81 | Open/615 | 9.08 | **415/673/940** | 1.02 | **415/615** | 1.04 |
| **415/673/940** | 2.37 | Open/870 | 2.95 | Open/615/940 | 8.99 | Open/500 | 9.18 | Open/415/615 | 1.03 | 415/673 | 1.06 |
| 615/673/940 | 2.41 | Open/673 | 3.15 | Open/500/870 | 9.02 | Open/940 | 9.40 | 415/500/615 | 1.03 | Open/415 | 1.29 |
| 500/673/940 | 2.42 | 615/940 | 3.56 | Open/415/500 | 9.03 | Open/415 | 9.43 | 415/615/673 | 1.03 | Open/500 | 1.36 |
| 673/870/940 | 2.42 | Open/615 | 3.70 | Open/500/673 | 9.06 | Open/870 | 9.48 | Open/415/940 | 1.04 | 500/940 | 1.38 |
| Open/870/940 | 2.43 | Open/415 | 4.03 | Open/415/615 | 9.08 | Open/673 | 9.94 | 415/500/673 | 1.04 | 500/870 | 1.41 |
| 615/870/940 | 2.43 | 870/940 | 4.23 | Open + 9 more two-filter combinations[1] | 9.08...9.43 | **500/870** | 14.67 | 415/615/870 | 1.04 | 415/500 | 1.53 |
| 415/870/940 | 2.53 | Open/940 | 4.27 | **500/870/940** | 10.41 | 673/940 | 15.42 | 415/615/940 | 1.04 | 500/615 | 1.55 |
| Open/500/615 | 2.57 | Open/500 | 4.29 | 615/870/940 | 11.08 | 415/870 | 16.61 | 415/673/870 | 1.04 | 500/673 | 1.55 |
| 500/870/940 | 2.61 | 500/940 | 5.32 | 673/870/940 | 12.64 | 615/870 | 18.38 | Open/415/673 | 1.05 | 415/870 | 1.58 |

A widely used commercial instrument for measuring all three solar components is the silicon-cell-based Rotating Shadowband Radiometer (RSR, www.irradiance.com). As explained earlier, the unfiltered silicon diode channel in the MFRSR is similar to, but not the same as the silicon diode pyranometer used in this instrument, specifically, the MFRSR's open-channel is temperature stabilized, responds to the additional wavelengths between 300 and 400 nm, and the solar components are corrected for cosine response. However, the instruments are similar enough that the procedures outlined in this paper should be useful in improving the measured irradiance components of this popular, multicomponent radiometer. A noteworthy finding was that a single calibration constant for the open-channel should not be used for both total and direct irradiance. We found that the direct normal irradiance calibration constant is generally 2–3% lower than that for total horizontal irradiance.

In the procedure described in this paper each component's calibration is determined from side-by-side comparisons with first-class thermopile instrumentation. It is useful to monitor the calibration stability of the MFRSR in the field between calibrations. Michalsky et al. (2001) and Augustine et al. (2008) describe in situ Langley calibration procedures for MFRSR measurements for aerosol optical depth applications. These calibrations are, in fact, extrapolations of the responses of the instrument to the top of the atmosphere (TOA), at least for the five filters centered near 415, 500, 615, 673, and 870 nm; typical uncertainties of these TOA responses are between 1 and 2%; this is not to say we obtain a 1–2% irradiance calibrations, which would have to include the added uncertainty in the extraterrestrial irradiance. If the filters used for the approximation of the broadband solar components included only these five filters, then the Langley calibrations could be used to track the stability of the instrument in the field.

The two channels that cannot be calibrated with the traditional Langley method are the open-channel and the 940-nm channel. It is evident from the top ten optimal combinations of channels for approximating broadband components listed in Table 3 that either the open-channel or the 940-nm channel, both of which include bands of water–vapor, is needed to explain the variance for most of the regressions for the total horizontal or direct normal irradiance approximations. Since all channels share the same diffuser, a logical assumption is that changes in diffuser transmission in the 415–870 nm channels can also be assumed for the 940-nm and open-channel. However, transmission changes in the 940-nm filter apart from the diffuser transmission changes would not be detected in this way. Michalsky et al. (1995) used a technique called the modified Langley method, first suggested by Reagan et al. (1987), to calibrate the 940-nm filter of an MFRSR. However, this method may not be feasible for most sites. For example, in north-central Oklahoma it took 14 months (Michalsky et al., 1995) to acquire enough modified-Langley plots to calculate the extraterrestrial response with 1% ($1\sigma$) uncertainty. In comparison, a filter channel without water can be calibrated to this accuracy with as little as 2 weeks of clear-sky data. The problem is that column water–vapor is highly unstable, even on clear days; therefore, the modified-Langley technique is of limited usefulness for tracking 940-nm stability. Lamp calibrations that simply measure the initial response and subsequent stability of this response would be a better proposition. Of course, if the MFRSR, which is used primarily for aerosol optical depth measurements, is located near a thermopile measurement set, as in the ARM program, then calibrations can be performed quasi-continuously as in this paper and the MFRSR used as a backup for the primary broadband solar measurements.

## Acknowledgments

The authors thank Chuck Long for creating the best estimate thermopile irradiance data product from the ARM central facility and for help in understanding how to use this product. The authors appreciate the insightful comments of three anonymous reviewers of our paper. The data used for this study were from the U.S. Department of Energy's Atmospheric Radiation Measurement Program's Climate Research Facility in north-central Oklahoma.

## References


Augustine, J.A., Hodges, G.B., Dutton, E.G., Michalsky, J.J., Cornwall, C.R., 2008. An aerosol optical depth climatology for NOAA's national surface radiation budget network (SURFRAD). J. Geophys. Res. 113, D11204. doi:10.1029/2007JD009504.

Harrison, L., Michalsky, J., Berndt, J., 1994. Automated multifilter rotating shadow-band radiometer: an instrument for optical depth and radiation measurements. Appl. Opt. 33, 5118–5125.

King, D.L., Myers, D.R., 1997. Silicon-photodiode pyranometers: operational characteristics, historical experiences, and new calibration procedures. In: 26th IEEE Photovoltaic Specialists Conference, September 29–October 3, Anaheim, California.

Michalsky, J.J., Harrison, L.C., LeBaron, B.A., 1987. Empirical radiometric correction of a silicon photodiode rotating shadowband pyranometer. Solar Energy 39, 87–96.

Michalsky, J.J., Liljegren, J.C., Harrison, L.C., 1995. A comparison of sun photometer derivations of total column water vapor and ozone to standard measures of same at the Southern Great Plains Atmospheric Radiation Measurement site. J. Geophys. Res. 100, 25995–26003.

Michalsky, J., Schlemmer, J., Berkheiser III, W., Berndt, J., Harrison, L., Laulainen, N., Larson, N., Barnard, J., 2001. Multi-year measurements of aerosol optical depth in the Atmospheric Radiation Measurement and Quantitative Links programs. J. Geophys. Res. 106, 12099–12107.

Reagan, J.A., Thome, K., Herman, B., Gall, R., 1987. Water vapor measurements in the 0.94 micron absorption band, In: Proceedings, International Geoscience and Remote Sensing Symposium, '87 Symposium, Ann Arbor, Michigan, IEEE, pp. 63–67.

Shi, Y., Long, C.N., 2002. Best estimate radiation flux value added product: algorithm operational details and explanations, Atmospheric Radiation Measurement Program Technical Report, ARM TR-008, 58 pp.